Neurocomputing 135 (2014) 180–191

Contents lists available at ScienceDirect

Neurocomputing

journal homepage: www.elsevier.com/locate/neucom

Integration of multiple orientation and texture information for finger-knuckle-print verification

Guangwei Gao [a,b], Jian Yang [a,b,*], Jianjun Qian [b], Lin Zhang [c]

[a] Institute of Advanced Technology, Nanjing University of Posts and Telecommunications, Nanjing, China
[b] School of Computer Science and Engineering, Nanjing University of Science and Technology, Nanjing, China
[c] School of Software Engineering, Tongji University, Shanghai, China

ARTICLE INFO

Article history:
Received 15 July 2013
Received in revised form
23 October 2013
Accepted 15 December 2013
Communicated by: Shiguang Shan
Available online 9 January 2014

Keywords:
Biometrics
Finger-knuckle-print
Orientation
Texture

ABSTRACT

The Competitive Coding (CompCode) scheme, which extracts and codes the local dominant orientation as features, has been widely used in finger knuckle print (FKP) verification. However, CompCode may lose some valuable information such as multiple orientation and texture of the FKP image. To remedy this drawback, a novel multiple orientation and texture information integration scheme is proposed in this paper. As compared with CompCode, the proposed scheme not only considers more orientations, but also introduces a multilevel image thresholding scheme to perform orientation coding on each Gabor filtering response. For texture features extraction, LBP maps are first obtained by performing Local Binary Pattern (LBP) operator on each Gabor filtering response, and then a similar coding scheme is applied on these LBP maps. Finally, multiple orientation and texture features are integrated via score level fusion to further improve FKP verification accuracy. Extensive experiments conducted on the PolyU FKP database show the effectiveness of the proposed scheme.

1. Introduction

Biometrics authentication is drawing more and more attention, and is much more preferable and reliable to those applications concerning high security, such as building access control, airport, e-banking, computer system login, and national ID card. In the past decades, researches have exhaustively studied various kinds of biometrics traits, including face, fingerprint, iris, palmprint, hand vein, voice, gait, etc. Furthermore, hand-based biometrics identifiers have been attracted considerable attention in the biometrics community. Techniques, such as palmprint [1–12], hand geometry [13], fingerprint [14–18], hand vein [19], have been developed and investigated in literature.

Recently, researchers have reported that finger-knuckle-print (FKP), the inherent skin pattern of the outer surface around the phalangeal joint of one's finger, is highly unique and can serve as a distinctive biometric identifier for online personal verification [12,20–29]. Fig. 1(a) shows the FKP image acquisition device and the use of the system in [20–24]. After an FKP image is captured (Fig. 1(b)), the region of interest (ROI) is extracted from it for feature extraction and matching. Fig. 1(c) and (d) shows the ROI of two FKP images from different fingers. One can see that FKP ROI images from different fingers have clear difference.

Both Feature extraction and matching also play important roles in FKP based verification system. In [20], Zhang et al. adopted the Gabor filter based competitive coding (CompCode) scheme, which was originally designed for palmprint recognition [2], to extract and code the local orientation information as FKP features. Later, this scheme was extended by combining the magnitude information extracted by Gabor filters [21]. In [22], the Fourier transform based band-limited phase only correlation (BLPOC) was adopted to extract the transform coefficients as the global features of FKP images for matching. In the local-global information combination (LGIC) scheme [23], the local orientation was taken as the local feature while the Fourier transform coefficients were taken as the global feature. This scheme achieved very promising accuracy for FKP verification. In [25], real Gabor filter was used to enhance the FKP image and then the scale invariant feature transform (SIFT) was applied to extract features. An adaptive steerable orientation coding (ASOC) scheme was proposed in [26], where high order steerable filters were first employed to extract continuous orientation feature map, and then the multilevel image thresholding method was used to code a FKP image. In [24], a set of phase congruency induced local features were defined. By fusing these local features in the matching score level, the proposed local feature integration (LFI) scheme led to much better results than other local feature based methods such as CompCode [20] and

* Corresponding author. Tel./fax: +86 25 8431 7297x307.
E-mail addresses: csggao@gmail.com (G. Gao), csjyang@mail.njust.edu.cn (J. Yang), qjjtx@126.com (J. Qian), cslinzhang@tongji.edu.cn (L. Zhang).

0925-2312/$ - see front matter © 2014 Elsevier B.V. All rights reserved.
http://dx.doi.org/10.1016/j.neucom.2013.12.036

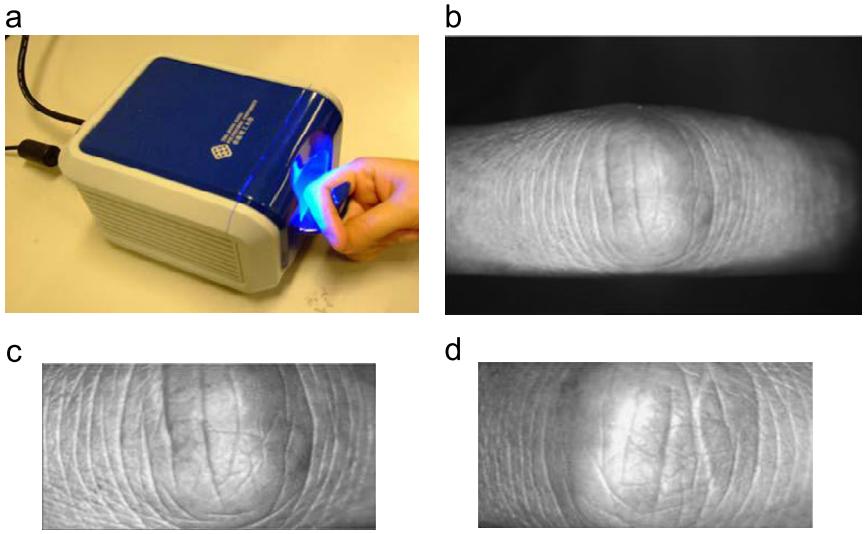

Fig. 1. (a) The FKP image acquisition device; (b) a typical FKP image; and(c), (d) two FKP ROI images from different fingers.

improved CompCode [21]. Recently, Riesz transforms are utilized to encode the local patterns of biometric images [12]. The experiments in [12] show that the proposed methods achieve quite similar verification accuracies with CompCode while need much less time at the feature extraction stage.

The orientation based coding approaches have many merits such as high accuracy, robustness to illumination variations and fast implementation. These algorithms share a common "competition" rule: the image is first convolved with several filters with different orientations. Then the "dominant" orientation is determined by some criterions. By simply coding the local orientation of the FKP, acceptable verification accuracy could be obtained with high matching speed. However, the line structures in FKP images are very complex. Multiple lines may intersect at some regions. If only one "dominant" orientation is extracted in these regions, much valuable discriminatory information will be lost.

To handle the aforementioned problems in traditional dominant orientation coding scheme, a novel multiple orientation coding scheme is first proposed in this paper. As compared with CompCode, the proposed method tries to use all the orientation information generated from the Gabor filtering responses rather than only "dominant" features. The multilevel image thresholding method [26] is introduced to perform orientation coding on each Gabor filtering response. Then all the coded maps are combined in the matching stage.

To the best of our knowledge, there is no investigation about texture information that has been reported for FKP verification in literature. We can make full use of this information to further improve the FKP verification accuracy. For texture feature coding, the conventional LBP [30] method is first performed on each Gabor filtering response, and then the similar thresholding based coding method is used on these LBP maps. Zhang et al. [11] pointed out that the fragile mask can be used for improving palmprint verification performance. A location in a palmprint's code map is consistent if it has the same value for most images of that palmprint; otherwise, it is fragile. In this paper, we find that the fragile location is also existed in FKP images. Therefore, in coding stage, fragile masks are evaluated and used. For matching, the modified Hamming distance is calculated by masking out these fragile locations. The texture information can bring complementary discrimination for improving FKP verification performance. We thus integrate the multiple orientation and texture information via score level fusion.

Comparative experiments on the PolyU finger-knuckle-print database [31] show that the proposed multiple orientations coding scheme can obtain comparative performance with state-of-the-art methods and the proposed integration scheme, which integrates orientation and texture information, can further improve the verification accuracy.

The rest of this paper is organized as follows. Section 2 briefly reviews the CompCode scheme and indicates its problems. Section 3 presents the proposed feature extraction, matching and the integration scheme. Section 4 performs extensive experiments, and Section 5 concludes the paper.

2. Brief review of competitive coding (CompCode)

Gabor filters have been widely used for extracting orientation or edge information in face, iris, fingerprint, palmprint, as well as FKP verification systems. A 2D Gabor filter is usually defined as

$$G(x,y)=\exp\left(-\frac{1}{2}\left(\frac{x'^2}{\sigma_x^2}+\frac{y'^2}{\sigma_y^2}\right)\right)\cdot\exp(i2\pi f x') \tag{1}$$

where $x'=x\cdot\cos\theta+y\cdot\sin\theta$, $y'=-x\cdot\sin\theta+y\cdot\cos\theta$, f is the frequency of the sinusoid factor, θ is the orientation of the normal to the parallel stripes, and σ_x and σ_y are the standard deviations of the 2D Gaussian envelop.

Let G_R be the real part of a Gabor filter, and I_{ROI} be an FKP ROI (region of interest) image. With a bank of Gabor filters sharing the same parameters, except the parameter orientation, at each location $I_{ROI}(x,y)$, the dominant orientation feature can be extracted and coded as follows:

$$CompCode(x,y)=\arg\min_j\{I_{ROI}(x,y)*G_R(x,y,\theta_j)\} \tag{2}$$

where $*$ stands for the convolution operation, and $\theta_j=j\pi/6$, $j=\{0,\ldots,5\}$. Obviously, each $CompCode(x,y)$ is assigned as an integer within 0–5.

For matching two CompCode maps P and Q, the normalized Hamming distance based angular distance is commonly adopted [2]:

$$d=\frac{\sum_{x=1}^{Rows}\sum_{y=1}^{Cols}h(P(x,y),Q(x,y))}{3S} \tag{3}$$

where S is the area of the code map, and

$$h(\alpha,\beta) = \min(|\alpha-\beta|, 6-|\alpha-\beta|), \quad \alpha,\beta \in \{0,\ldots,5\} \tag{4}$$

By using the "min" rule, CompCode only uses one "dominant" orientation, which may lose some discriminative information in intersectant region with many lines.

3. Multiple orientation and texture feature extraction

3.1. Motivation

The CompCode scheme has merits of simplicity and speediness, and leads to acceptable accuracy in FKP verification [20,21,23]. For coding, 6 Gabor filtering responses are competed through the "min" rule, resulting in only one "dominant" orientation. The code value is assigned as the orientation along which the smallest response is obtained. However, multiple lines may intersect at some regions of the FKP image. Such "dominant" based method may lose much valuable structural information for FKP verification. Fig. 2(a) and (b) shows an example region where multiple lines intersect. Fig. 2(c) plots the curve of Gabor filtering response versus orientation for the local region in Fig. 2(b). We can see that several valleys imply several orientations in this local region. If only one orientation is kept, much valuable discriminatory information will be lost.

As illustrated in Section 2, a bank of Gabor filters with different orientations is convolved with the FKP image. Since we want to keep the multi-orientation characteristics of FKP images, one intuitive idea is to fully capture all the 6 Gabor filtering responses. For each filtering response, we can use some rule to code it. These 6 coded responses are then combined together for matching. In addition, the texture information can be incorporated into our proposed scheme, which may provide additional discrimination for FKP verification. In the following subsection, we will first introduce the strategy for extracting and matching the multiple orientation and texture features. Then, a simple yet useful score level fusion scheme is introduced to fuse them.

3.2. Multiple orientation coding (MoriCode) for orientation feature extraction

Let $R_j = I_{ROI} * G_R(\theta_j)$ be the Gabor filtering response of an FKP ROI image I_{ROI} to the jth ($j=0,1,\ldots,5$) Gabor filter with orientation θ_j, as defined in Eq. (1). In the proposed scheme, all these 6 responses are fully used, differing from that in CompCode. Both considerable storage and significant computational cost are needed when directly using of these continuous responses for FKP representation and matching. Thus, a quantization method is required for filtering response coding.

The quantization on a single filtering response image can be regarded as a multilevel image thresholding process. A key issue for multilevel thresholding is the determination of the multi-thresholds, and histogram based self-adaptive (HSA) technique is widely used for this task. Without loss of generality, let's focus on the multi-thresholds learning on response R_0. The multi-thresholds learning of other response maps can be conducted similarly. Let N be the number of response classes, $C_1, C_2,\ldots,C_N$ be the corresponding classes and $r_1, r_2,\ldots,r_{N-1}$ be the thresholds needed to be learned respectively. Let us define class $C_k = \{\varphi | \varphi \in [r_{k-1}, r_k]\}$, where $k \in [2\ldots N-1]$. C_1 and C_N are defined as $C_1 = \{\varphi | \varphi \in [\min(R_0), r_1]\}$, $C_N = \{\varphi | \varphi \in (r_{N-1}, \max(R_0)]\}$, where $\min(R_0)$ and $\max(R_0)$ are the minimum and maximum of filtering response R_0.

The histogram $h(\varphi)$ shows occurrences frequency of the response φ in the response map, and the normalized histogram is denoted as $p(\varphi) = h(\varphi)/S$ with S the size of response map. Fig. 3(d) shows the histogram of filtering response in Fig. 3(b) (denoted as red dotted lines). For the kth ($k \in [2\ldots N-1]$ response class C_k, statistical properties such as the probability of the class, the mean and the variance of the class can be computed as $w_k = \sum_{\varphi \in C_k} p(\varphi)$, $\mu_k = \sum_{\varphi \in C_k} (p(\varphi)\cdot\varphi / w_k)$ and $\sigma_k^2 = \sum_{\varphi \in C_k} (p(\varphi)\cdot(\varphi-\mu_k)^2 / w_k)$. The optimal

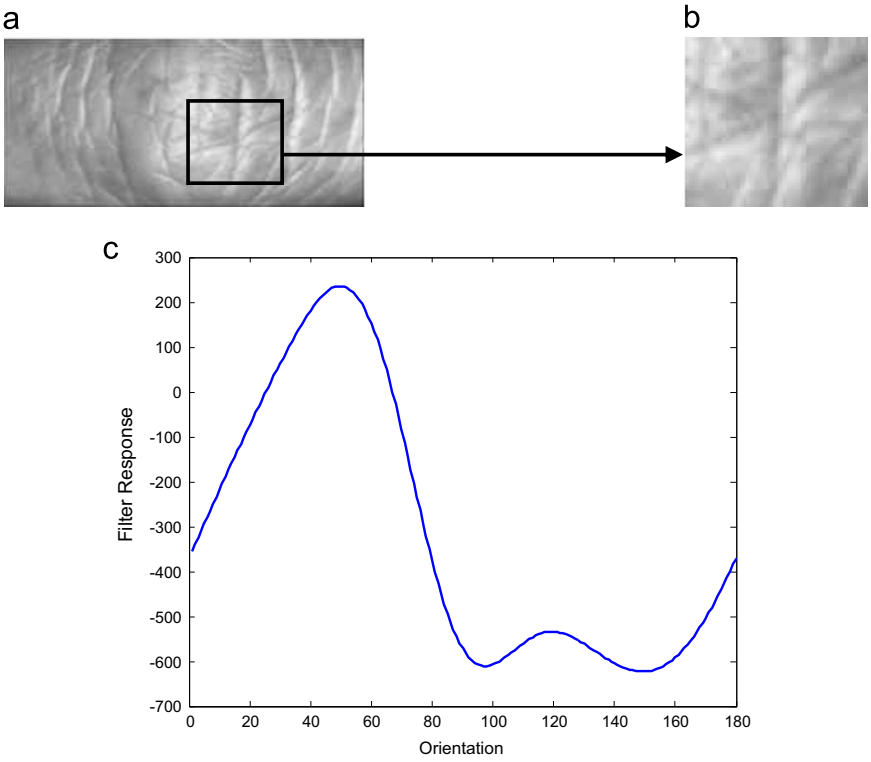

Fig. 2. (a) An FKP ROI image; (b) cropped and enlarged images with intersected lines; and (c) Gabor filtering responses versus orientation.

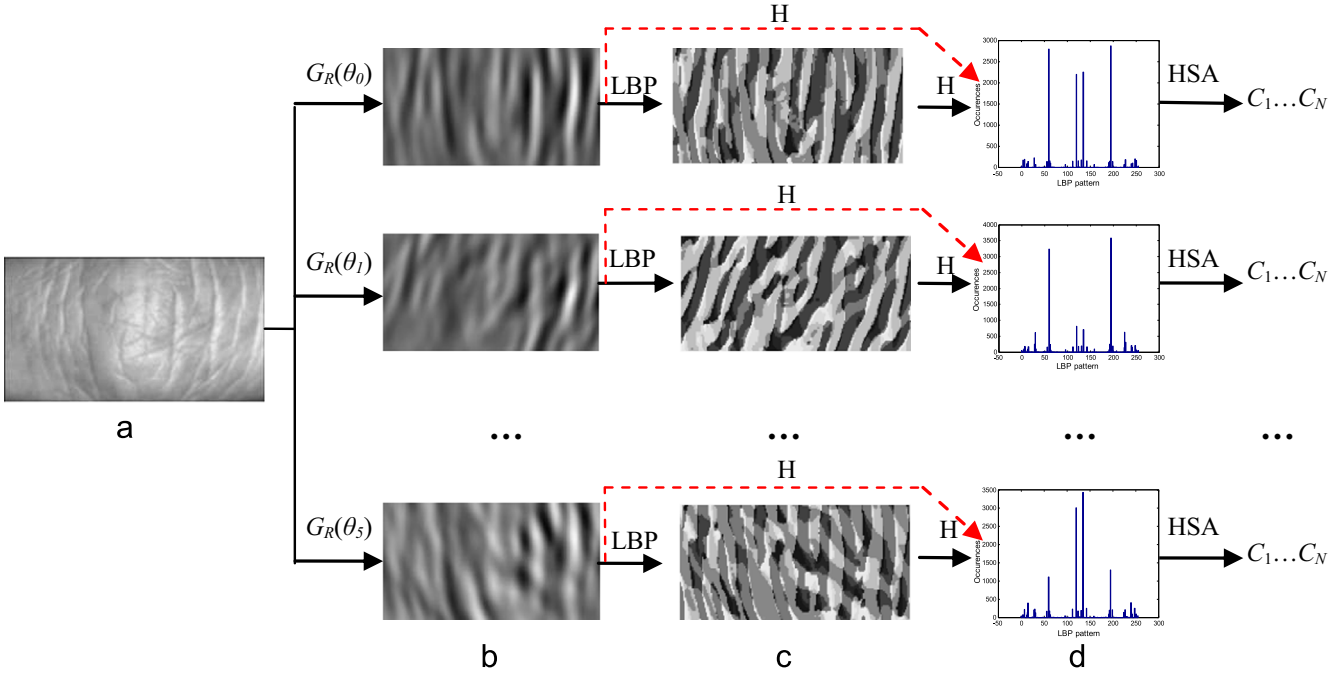

Fig. 3. (a) An FKP ROI image; (b) its six Gabor filtering responses; (c) the corresponding LBP map of the responses in (b); and (d) the corresponding histogram of the map in (b) or (c). (For interpretation of the references to color in this figure caption, the reader is referred to the web version of this paper.)

multi-thresholds are found by minimizing the following criterion called within-class variance:

$$[r_1^*, r_2^*, \ldots, r_{N-1}^*] = \arg\min\left(\sum_{k=1}^{N} w_k \sigma_k^2\right) \tag{5}$$

DP-SMAWK algorithm presented in [32] is employed to find the optimal thresholds (i.e. r_1^*, r_2^*,…,r_{N-1}^*), and then the optimal classes are C_1^*, C_2^*,…,C_N^*. It should be noted that for each response map R_j, we can get different optimal classes duo to the difference of the corresponding response histogram.

After obtaining the optimal classes C_1^*, C_2^*,…,C_N^* for each response map, the quantization is then performed on the original response map for orientation feature coding. For each response value α in the response map, its final coded value is given as follows:

$$Code(\alpha) = \mathrm{mod}(\{k | [\alpha] \in C_k^*, 1 \le k \le N\}, N) \tag{6}$$

Obviously, the code value is within 0 to $N-1$. Some coded examples are shown in Fig. 4, where (a) and (b) are different images captured from the same class while (c) is an image taken from another different class. From Fig. 4(d)–(f), we can see that the codes from the same class have strong similarity, while the codes from different class have significant difference. The above observation indicates that the codes have strong discrimination. It should be noted that each image actually has 6 such code maps since 6 Gabor filters with different orientation are used.

3.3. Multiple texture coding (MtexCode) for texture feature extraction

Apart from the orientation features, the FKP images also have many finer texture features, which may convey power discriminative information. In this subsection, we will study the texture information contained in the FKP image in detail.

In [30], Local Binary Pattern (LBP) histogram was proposed for rotation invariant texture classification. LBP is a gray-scale texture operator which characterizes the spatial structure of the local image texture. It has also been successfully adapted to many applications, such as face recognition [33], dynamic texture recognition [34] and shape localization [35]. Given a central pixel in the image, a pattern number can be computed by comparing its value with those of its neighborhoods:

$$LBP_{P,R} = \sum_{p=0}^{P-1} s(g_p - g_c) 2^p, \quad s(x) = \begin{cases} 1, & x \ge 0 \\ 0, & x < 0 \end{cases} \tag{7}$$

where g_c is the gray value of the central pixel, g_p is the value of its neighbors, P is the number of neighbors and R is the radius of the neighborhood.

Suppose that the texture image is $N \times M$. After identifying the LBP pattern of each pixel (i, j), the whole texture image can be represented by a histogram:

$$H(k) = \sum_{i=1}^{N} \sum_{j=1}^{M} f(LBP_{P,R}(i,j), k), \quad k \in [0, K]$$
$$f(x,y) = \begin{cases} 1 & x = y \\ 0 & \text{other} \end{cases} \tag{8}$$

where K is the maximal LBP pattern value.

To fully use the texture information from the 6 Gabor filtering responses, like the work in [36], we conduct the LBP operator on each Gabor filtering response. Thus, each response map is converted to a LBP map. Fig. 3(c) shows examples of LBP maps for one FKP image with configurations of $P=8$, $R=1$.

After getting the LBP maps, HSA technique based multilevel image thresholding is also used for texture feature coding. The coding process is similar as that in Section 3.2. First, the LBP histogram is evaluated for each LBP map. Then, the DP-SMAWK algorithm presented in [32] is employed to find the optimal thresholds, and the optimal classes are C_1^*, C_2^*,…,C_N^*. It should be noted that the histograms in Section 3.2 are directly evaluated on the Gabor filtering responses, while in this section they are evaluated on the LBP maps. For each pattern α in the LBP maps, its final code value is given by Eq. (6). Some coded examples are

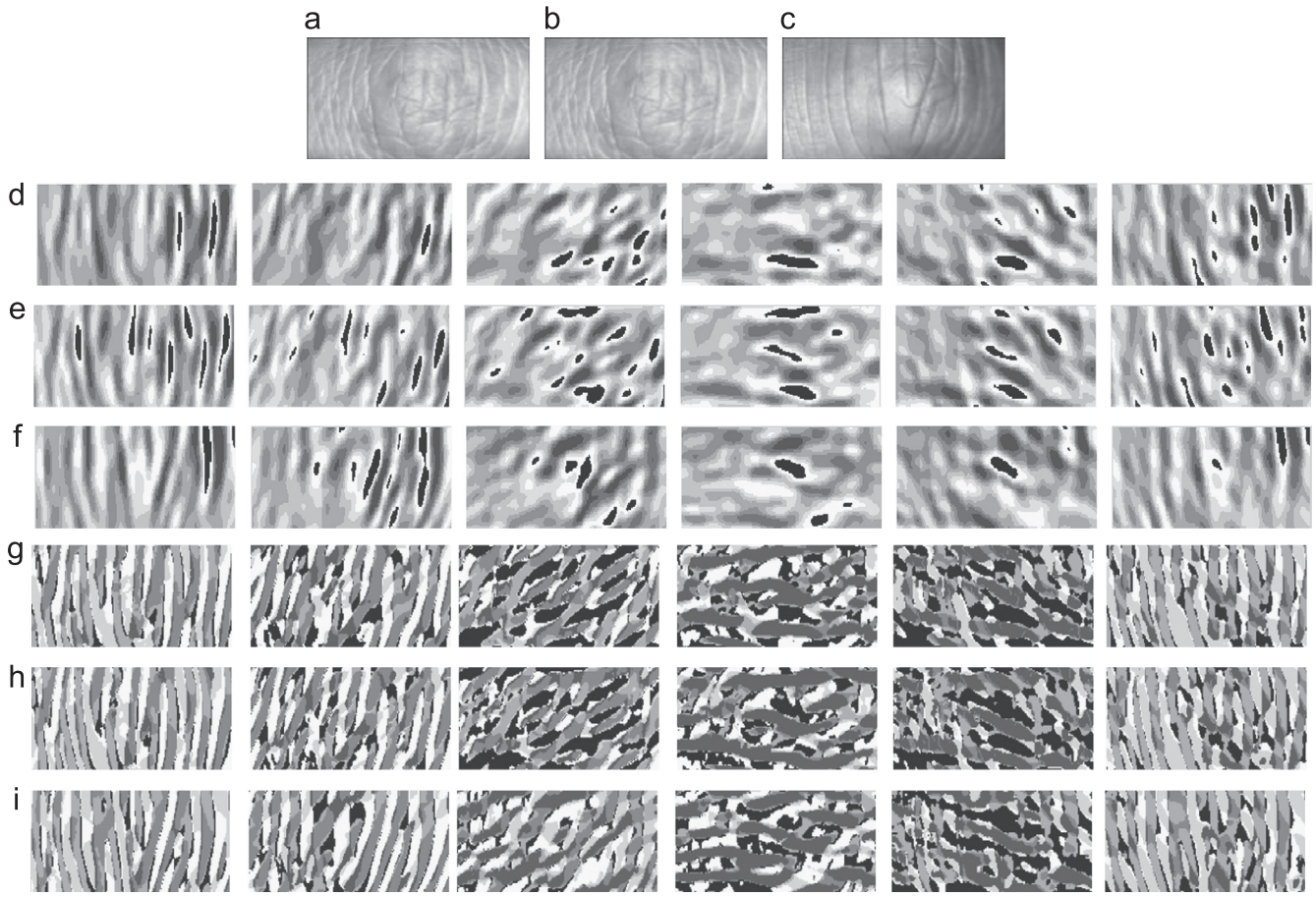

Fig. 4. (a) and (b) are the different images taken from the same class while (c) is taken from a different class; (d)–(f) are the 6 orientation coded maps for (a)–(c) respectively; (g)–(i) are the 6 texture coded maps for (a)–(c) respectively.

shown in Fig. 4(g)–(i), from which we can see that the proposed texture coding scheme can well characterize the texture information contained in the FKP image.

3.4. Feature matching

As well as CompCode, the normalized Hamming distance based angular distance is adopted for matching. Let P and Q be the MoriCode (MtexCode) maps of two FKP ROI images respectively. Their angular distance *MoriD* (*MtexD*) can be computed as follows:

$$MoriD\ (MtexD) = \frac{\sum_{x=1}^{Rows}\sum_{y=1}^{Cols}\sum_{j=0}^{5} G(P_j(x,y), Q_j(x,y))}{6\cdot(N/2)\cdot S} \tag{9}$$

where P_j (Q_j) is the jth code map of P(Q), S is the area of the code map and $G(\alpha,\beta)$ is defined as Eq. (4):

$$G(\alpha,\beta) = \min(|\alpha-\beta|, N-|\alpha-\beta|), \quad \alpha,\beta \in \{0,\ldots,N-1\} \tag{10}$$

Obviously, *MoriD* (*MtexD*) is between 0 and 1. To overcome imperfect preprocessing, multiple matches are performed by translating one set of features in horizontal and vertical directions. The ranges of the horizontal and the vertical translations are empirically set as -9 to 9 and -4 to 4 in this paper.

For a specific location in the Gabor filtering response, if its response has a large magnitude, the corresponding location will likely be consistent (i.e., have much orientation information). On the contrary, if the response is close to zero, the corresponding location will likely be fragile (i.e., have less orientation information). These fragile locations will contribute less to the matching, and in some cases may increase the matching distance of the images from the same class. If we can remove these locations in the matching stage, the matching accuracy can be improved. Two examples are shown in Fig. 5(a), where the locations with small response are marked with blue rectangle.

Based on the above analysis, we use a simple method to figure out the potential locations that have small response. Denote by R_j the filtering response of an FKP ROI image to the jth ($j=0,1,\ldots,5$) Gabor filter with orientation θ_j. The magnitude values contained in the matrix R_j can be sorted to identity p percent smallest ones. The locations containing p percent smallest magnitude values are considered fragile and represented as zeros while others are considered consistent and represented as ones. We use a separate matrix named fragility mask f_j to store the value one and zero. Thus, f_j (x,y) indicates whether the value R_j (x,y) is consistent or not. Examples of fragility masks are shown in Fig. 5(d). For comparison, we also show the corresponding response R_j. In Fig. 5(b), the first two are different images captured from the same class while the last two are images captured from another different class. The images are convolved with $G_R(\theta_0)$. It needs to be noted that each image actually has 6 such fragility masks since 6 Gabor filters are used and $p=25\%$.

Eq. (9) gives equal weight for all locations in a code map. However, not all of the locations in a code map are equally useful. According to this consideration, we try to mask out these less useful locations when compute the Hamming distance. With this modification, the matching in a comparison is based on fewer locations, but each location used is more important.

The modified Hamming distance can be computed as follows. Suppose that P and Q are two Moricode (MtexCode) maps. Their

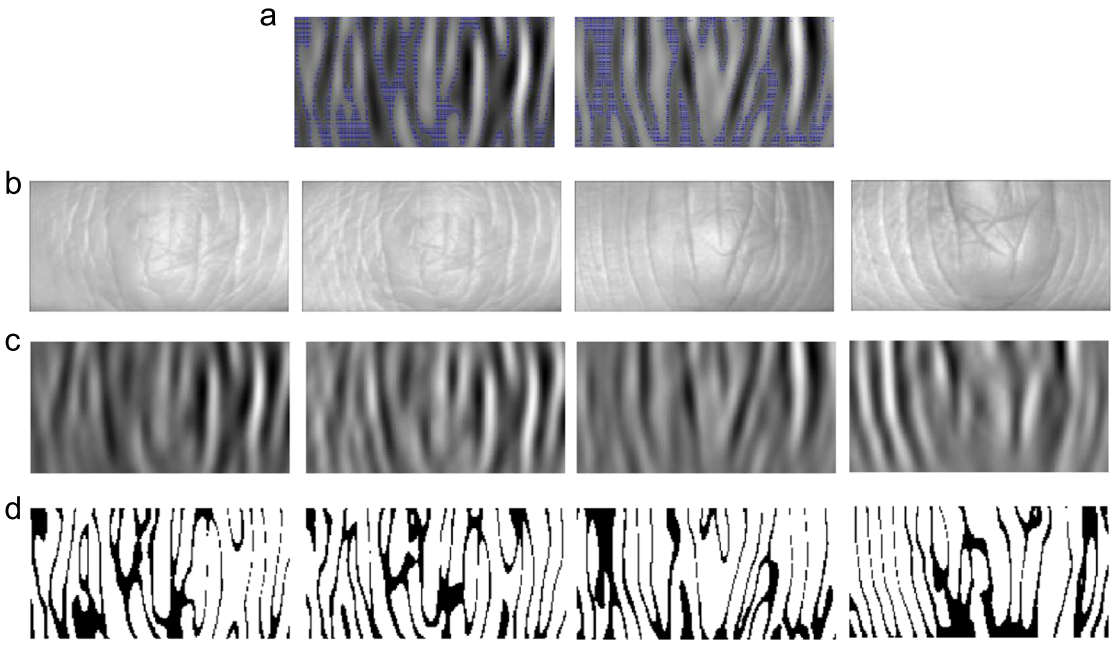

Fig. 5. (a) The marked locations with small response; (b) the first two are different images taken from the same class while the last two are taken from another different class; (c) The corresponding filtering responses for (b); and (d) The corresponding fragility masks for (c). (For interpretation of the references to color in this figure caption, the reader is referred to the web version of this paper.)

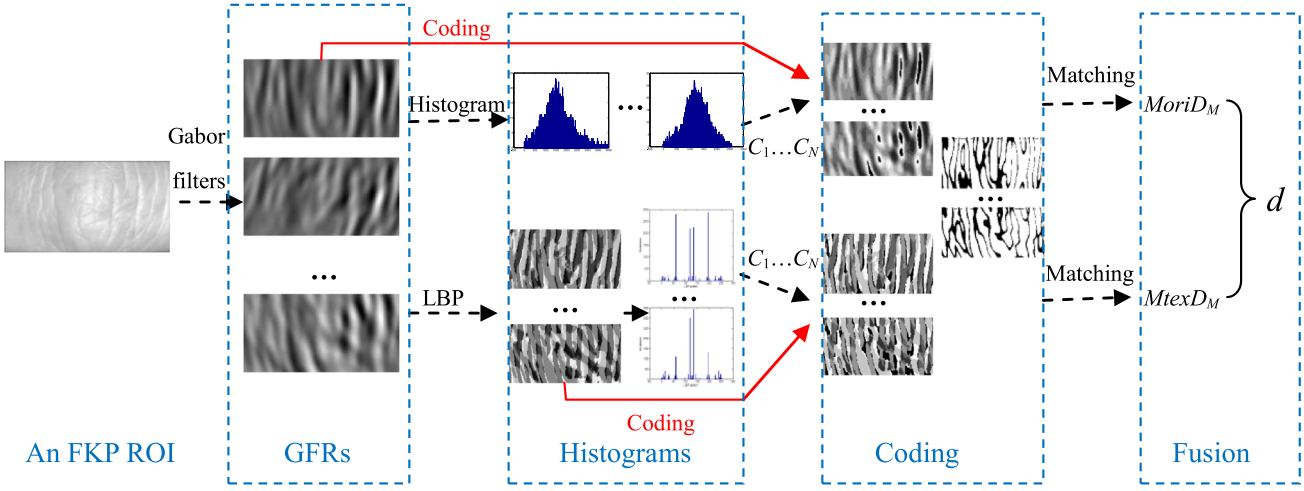

Fig. 6. Framework of the proposed multiple orientation and texture integration scheme.

fragility mask matrices are f and g, respectively. Then, the modified Hamming distance, denoted by $MoriD_M$ ($MtexD_M$), is defined as

$$MoriD_M\ (MtexD_M) = \frac{\sum_{x=1}^{Rows}\sum_{y=1}^{Cols}\sum_{j=0}^{5} G(P_j(x,y), Q_j(x,y)) \cap (f_j(x,y) \cap g_i(x,y))}{6 \cdot (N/2) \cdot \sum_{x=1}^{Rows}\sum_{y=1}^{Cols} f_j(x,y) \cap g_i(x,y)} \quad (11)$$

where P_j (Q_j) is the jth code map of $P(Q)$, f_j (g_j) is the jth mask of $f(g)$, $G(P_j,Q_j)$ is defined as Eq. (10), and $\cap$ means the bitwise "AND" operation.

3.5. Integration of orientation and texture Features

The two features described in Sections 3.2 and 3.3 reflect different local information contained in an FKP image. Thus, we can expect higher verification accuracy by assembling information from the two features together, which can be achieved by a score level fusion. Suppose that we have obtained the matching distance $MoriD_M$ and $MtexD_M$ by matching the multiple orientation and texture features of two images respectively. The two distances can be fused together to get the final matching distance.

There are a lot of rules for fusion, such as the Simple-Sum (SS) rule, the MIn-Score (MIS) rule, the MAx-Score (MAS) rule and the Matcher-Weighting (MW) rule [37]. In our case, $MoriD_M$ and $MtexD_M$ can be considered to be obtained from two different matchers, matcher 1 (multiple orientation based matcher) and matcher 2 (multiple texture based matcher). We use the MW rule in this paper. In the MW rule, weights are assigned according to the equal error rate (EER) obtained on a training dataset by different matchers. Denote by e_k the EER of the two matchers, $k=1,2$. Then, the weights corresponding to matcher k can be calculated as follows:

$$w_k = \left(1 / \sum_{k=1}^{2} \frac{1}{e_k}\right) / e_k \quad (12)$$

where $0 \le w_k \le 1$ and $w_1 + w_2 = 1$. Obviously, weights are inversely proportional to the corresponding EERs. Then, the final matching

distance integrating orientation and texture features is calculated as

$$d = w_1 \cdot MoriD_M + w_2 \cdot MtexD_M \quad (13)$$

3.6. Summary of the proposed method

In Sections 3.2 and 3.3, we fully capture the multiple orientation and texture information for feature coding and matching. In the proposed method, an FKP image is modeled by the following steps: (1) An input FKP ROI image is transformed to obtain multiple Gabor filtering responses (GFRs) by applying multi-orientation Gabor filters; (2) Histograms are evaluated to obtain optimal multi-thresholds. For orientation feature extraction, the histogram is calculated directly on GFRs. While for texture feature extraction, each GFR is first converted to LBP map, then histogram is evaluated based on these LBP maps; (3) Multilevel image thresholding based coding is performed on GFRs and LBP maps based on the optimal multi-thresholds respectively. Meanwhile, fragility masks are evaluated. The overall framework of the proposed approach is illustrated in Fig. 6.

4. Experimental results and discussions

4.1. FKP database and the test protocol

In the previous work [20–24,31], an FKP database was established. This database consists of the cropped FKP region of interest (ROI) images of 4 fingers (the left index, the left middle, the right index and the right middle) from 165 volunteers. Each finger knuckle was asked to provide 12 samples from two separated sessions with 6 samples per session, giving a total of $165 \times 4 \times 12 = 7920$ samples from 660 (i.e., 165×4) fingers. The images from the first session were taken as gallery set while the images from the second session were taken as the probe set. To obtain statistical results, each image in the probe set was used to match all the images in the gallery set. A genuine matching was counted if the two images come from the same finger; otherwise, an imposter matching was counted.

The equal error rate (EER), which is the point when the false accept rate (FAR) is equal to the false reject rate (FRR), is used to evaluate the verification accuracy. The decidability index d [38] is used to measure how well the genuine and the imposter distance are separated. Denote the mean of the genuine (imposter) matching distances as μ_1 (μ_2), the standard deviation of the genuine (imposter) matching distances as σ_1 (σ_2), d is defined as follows:

$$d = \frac{|\mu_1 - \mu_2|}{\sqrt{(\sigma_1^2 + \sigma_2^2)/2}} \quad (14)$$

Furthermore, by adjusting the matching threshold, a detection error tradeoff (DET) curve, which is a plot of false rejection rates (FRR) against false acceptance rates (FAR) for all possible thresholds, is vividly used to evaluate the overall verification accuracy of the system.

4.2. Determination of the parameters

In our proposed method, the quantization number N, the number of neighbors P (or the radius of the neighborhood R) and the percent p need to be tuned. Parameters were tuned based

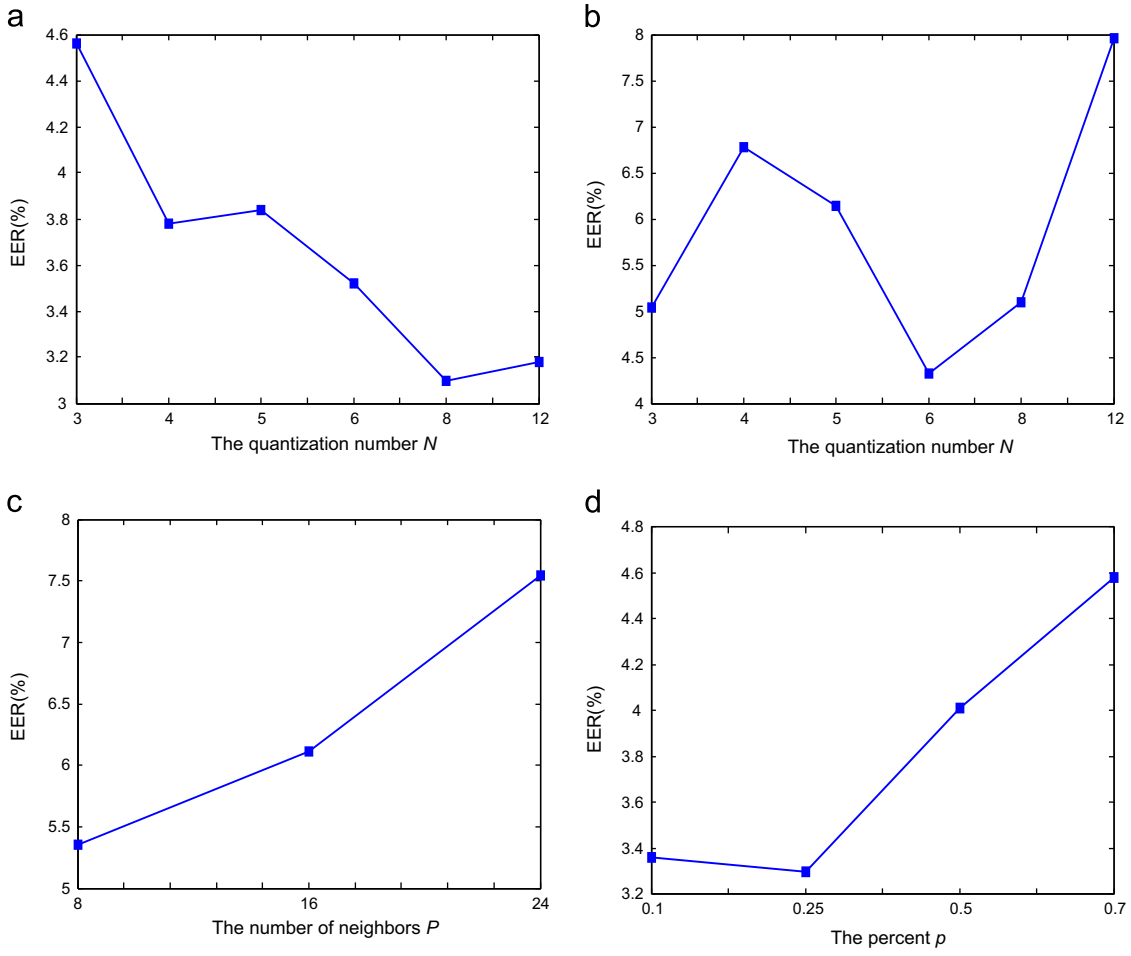

Fig. 7. EER versus different parameter settings: (a) and (b) The quantization number N; (c) the number of neighbors P; and (d) the percent p.

on a sub-dataset containing images from the first 165 FKP fingers and the tuning criterion was that parameters that led to a lower EER would be chosen. Fig. 7 shows the EER value versus different parameter settings performed on R_0 for illustration. Thus, the parameters used in this paper were set as $N=8$ for orientation coding, $P=8$, $R=1$, $N=6$ for texture coding and $p=25\%$. Moreover, fusion weights w_1 and w_2 can be calculated using Eq. (12).

4.3. Effectiveness of the fragility masks

We will compare the verification accuracies obtained by using *MoriD*, $MoriD_M$ and *MtexD*, $MtexD_M$ respectively to verify the effectiveness of the fragility masks. Experiments are conducted on a sub-dataset containing the first 165 FKP fingers.

The EER and *d* are listed in Table 1. From the results we can see that by masking out fragile locations in code maps, the EER could be reduced from 1.782% to 1.413% and 2.305% to 2.243%. The drop of EER is 20.71% ((1.782 − 1.413)/1.782) and 2.69% ((2.305 − 2.243)/2.305), which demonstrates that the verification accuracy could be significantly improved by using the fragility masks.

Table 1
EER (%) and *d* by different schemes.

Method	EER	*d*
MoriD	1.782	4.1214
***MoriD*$_M$**	**1.413**	**4.4538**
MtexD	2.305	3.2225
***MtexD*$_M$**	**2.243**	**3.2891**

Table 2
EER (%) and *d* by different schemes in experiment 1.

Method	EER	*d*
CompCode[20]	1.386	4.4302
BOCV[6]	1.833	4.1251
ImCompCode&MagCode[21]	1.210	4.5224
MoriCode	1.201	**4.7321**
MtexCode	1.816	3.4520
MoriCode&MtexCode	**1.048**	4.4014

4.4. FKP verification results

In order to show and explain the performance of the proposed scheme clearly, 3 experiments were conducted. We evaluated and compared the performance of some state-of-the-art coding-based feature extraction methods: CompCode [20], BOCV [6], ImCompCode&MagCode [21] and the proposed MoriCode&MtexCode. Gabor filters used in CompCode, BOCV, ImCompCode&MagCode and the proposed MoriCode&MtexCode were all of the form (1). Also, for MoriCode, MtexCode and MoriCode&MtexCode, $MoriD_M$ and $MtexD_M$ are used.

4.4.1. Experiment 1

In the first experiment, all classes of FKPs were used. Therefore, there were 660 (165×4) classes and 3960 (660×6) images in the gallery set and the probe set each in this experiment. Each image in the probe set was matched against all the images in the gallery set. Thus, the number of genuine matchings and imposter matchings are 23,760 and 15,657,840, respectively. The verification accuracy is given in Table 2. The DET curves obtained by using each evaluated methods are shown in Fig. 8(a).

From the experimental results shown in Table 2 and Fig. 8(a), the following findings can be made. First, the MoriCode scheme performs much better than the MtexCode scheme. Second, since MoriCode could keep more orientation information than CompCode, it could get better results than CompCode. Third, the MoriCode&MtexCode scheme which integrates the multiple orientation and texture information performs obviously better than using any of them individually. This is because the texture information can provide complementary discrimination. Distance distributions of genuine matchings and imposter matchings obtained by the proposed scheme are plotted in Fig. 8(b).

4.4.2. Experiment 2

As mentioned in Section 4.1, the FKP database contains images from four types of fingers: left index fingers, left middle fingers, right index fingers and right middle fingers. For each type of FKPs, the probe and the gallery each contains 165 classes and 990 (165×6) images, and the number of genuine and imposter matchings are 5940 and 974,160, respectively. DET curves for different finger types and different verification methods are shown in Fig. 9. Experimental results in terms of EER and *d* are summarized in Table 3 for comparison.

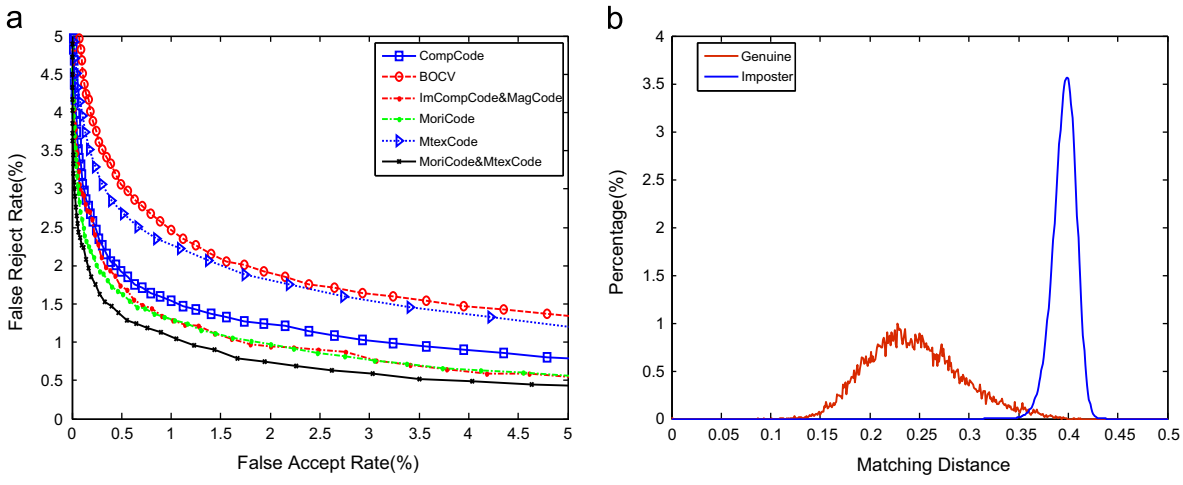

Fig. 8. (a) DET curves for experiment 1 by different schemes; (b) distance distribution of genuine matchings and imposter matchings with the proposed MoriCode&MtexCode in experiment 1.

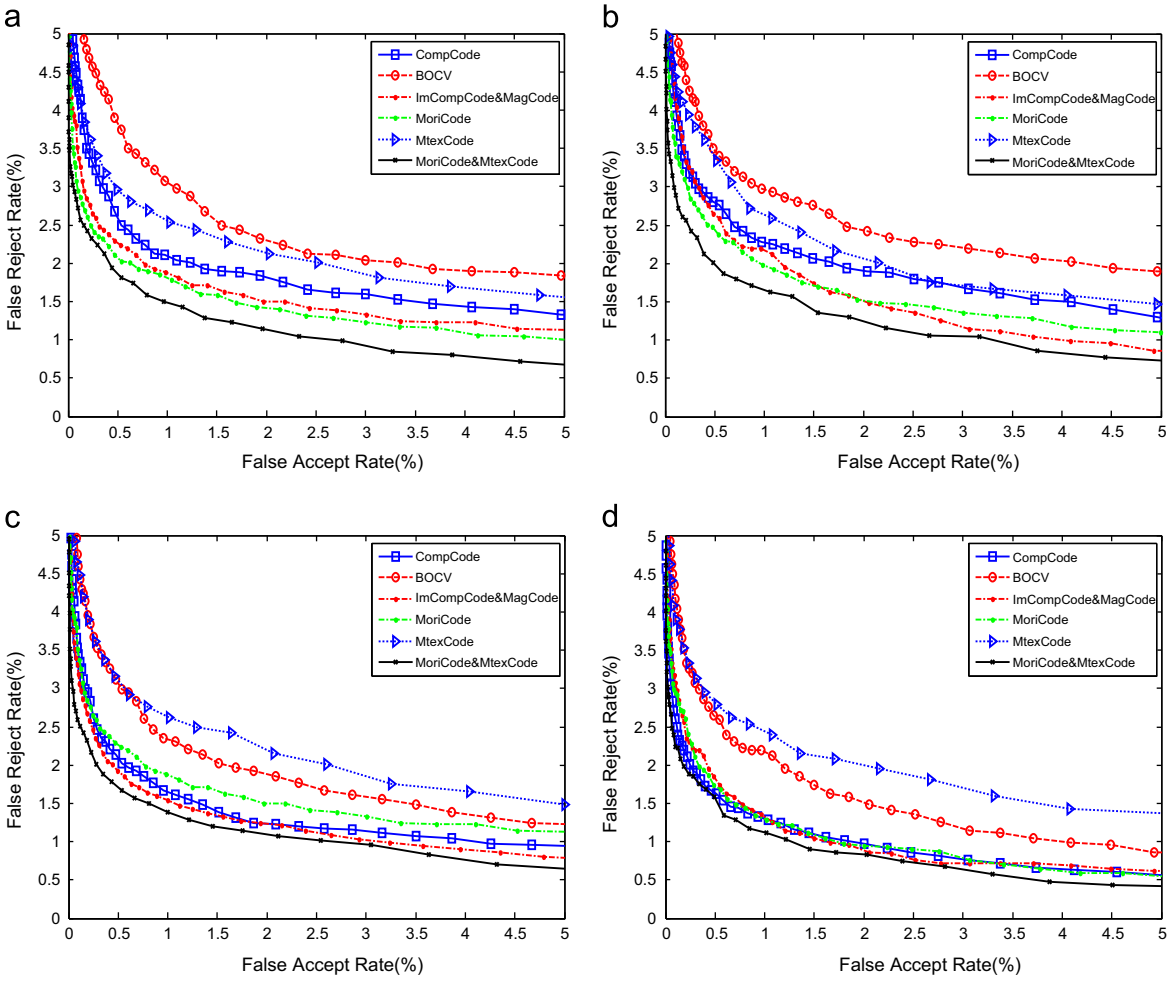

Fig. 9. DET curves for FKPs from (a) left index fingers; (b) left middle fingers; (c) right index fingers; and (d) right middle fingers.

Table 3
EER (%) and *d* by different schemes in experiment 2.

Method	*Left index*		*Left middle*		*Right index*		*Right middle*	
	EER	*d*	EER	*d*	EER	*d*	EER	*d*
CompCode[20]	1.884	4.2167	1.883	4.4005	1.445	4.2599	1.175	4.4316
BOCV[6]	2.202	3.9873	2.299	3.3664	1.892	4.0342	1.647	3.9051
ImCompCode&MagCode[21]	1.610	4.3550	1.650	4.4325	1.326	4.3302	1.097	4.5224
MoriCode	1.544	**4.4565**	1.689	**4.5233**	1.605	**4.4550**	1.244	**4.6164**
MtexCode	2.077	3.4257	2.078	3.4649	2.115	3.3222	2.055	3.4338
MoriCode&MtexCode	**1.328**	4.1174	**1.453**	4.0718	**1.247**	3.9427	**1.063**	4.1989

From the experimental results, we can see that for left fingers, the proposed MoriCode scheme performs obviously better than CompCode, BOCV and ImCompCode&MagCode. For right fingers, the proposed MoriCode scheme has similar performance with CompCode. By integrating the multiple orientation and texture information, the proposed MoriCode&MtexCode scheme has the best performance among all of the listed methods in all types of fingers in terms of EER. The drop of EER is 29.51%, 22.84%, 13.70% and 9.53% respectively, which clearly clarify the superiority of the proposed MoriCode&MtexCode.

4.4.3. *Experiment 3*

In Sections 4.4.1 and 4.4.2, we only list the fused results obtained by using MW rule. In this subsection, we compared the performance of the commonly used MIN, MAX, SS and MW rules.

Table 4
EER (%) and *d* by different schemes in experiment 3.

Fusion rules	*All classes*	*Left index*	*Left middle*	*Right index*	*Right middle*
MIN	1.201	1.544	1.689	1.605	1.244
MAX	1.775	2.059	2.066	2.092	2.042
SS	1.128	1.404	1.481	1.310	1.096
MW	**1.048**	**1.328**	**1.453**	**1.247**	**1.063**

The bold font indicates the best results.

The EER values obtained by using different fusion rules are listed in Table 4. From Table 4, we can see that the lowest EER is obtained by the MW rule. The MW rule uses more information with a training dataset, thus it works better than the MIN, NAX and SS rules.

4.5. Storage and speed

It should be noted that the proposed MoriCode&MtexCode scheme needs more storage space than CompCode. In the feature extraction stage, 6 convolutions are needed, which is also needed for CompCode. For each orientation, each feature point is represented by 4-bits for MoriCode and 3-bits for MtexCode. Thus 24-bits and 18-bits are used respectively. It is easy to see that MoriCode and MtexCode needs 8 times and 6 times storage compared with CompCode.

The FKP recognition software is implemented using the Visual C#.Net 2010 on a ASUS K42D PC embedded AMD N830 processor and 4 GB of RAM. The execution time for data preprocessing and ROI extraction is 128 ms. The time for MoriCode&MtexCode-based feature extraction and matching is 249 and 15 ms, respectively. The total execution time for one verification operation is less than 0.5 s, which is fast enough for real-time applications. We believe that with the optimization of the implementation, the system's efficiency could be much further improved.

4.6. Discussion

In section 4.4, we have evaluated the performance of the proposed MoriCode, MtexCode and MoriCode&MtexCode for all types of fingers. From the experimental results we found that MoriCode perform similarly with CompCode for right fingers.

The reason may be that left fingers have more intersected lines than that of right fingers. Fig. 10(a) shows four FKP ROI images from four types of finger respectively. To illustrate this more intuitively, we visualize the standard deviation (std) of the four types of finger as follows. For each type of fingers, we first count the std of the 6 Gabor filtering response for each FKP ROI image. Then the std of each type of fingers can be obtained. For a specific location, if it has intersected lines, the std for this location may be small and vice verse. The std for each type of fingers is visualized in Fig. 10(b)–(e), from which we can see that the std planes for left fingers (Fig. 10(b) and (c)) are relatively flatter than that of right fingers (see Fig. 10(d) and (e)), which demonstrate that the left fingers may have more intersected lines than that of right fingers. When MoriCode is performed on right fingers, the multi-orientation characteristics cannot be well revealed. Thus, MoriCode may have similar performance with CompCode. Conversely, the left fingers may have more intersected lines and MoriCode can well extract multi-orientation information while CompCode cannot. Thus, in such case, MoriCode performs better than CompCode.

5. Conclusions

This paper presents a novel multiple orientation and texture information integration scheme for finger-knuckle-print (FKP) verification. For an input query image, its 6 Gabor filtering responses are obtained. For multiple orientation feature extraction, each Gabor filtering response is directly coded by using multilevel image thresholding based quantization technique. For texture feature extraction, Local Binary Pattern (LBP) operator is first performed on these Gabor filtering responses and then multilevel image thresholding based quantization technique is used on the LBP maps. The texture information can provide extra discrimination for improving FKP verification performance. For feature matching, the fragility masks, which mask out the locations that have small responses, are

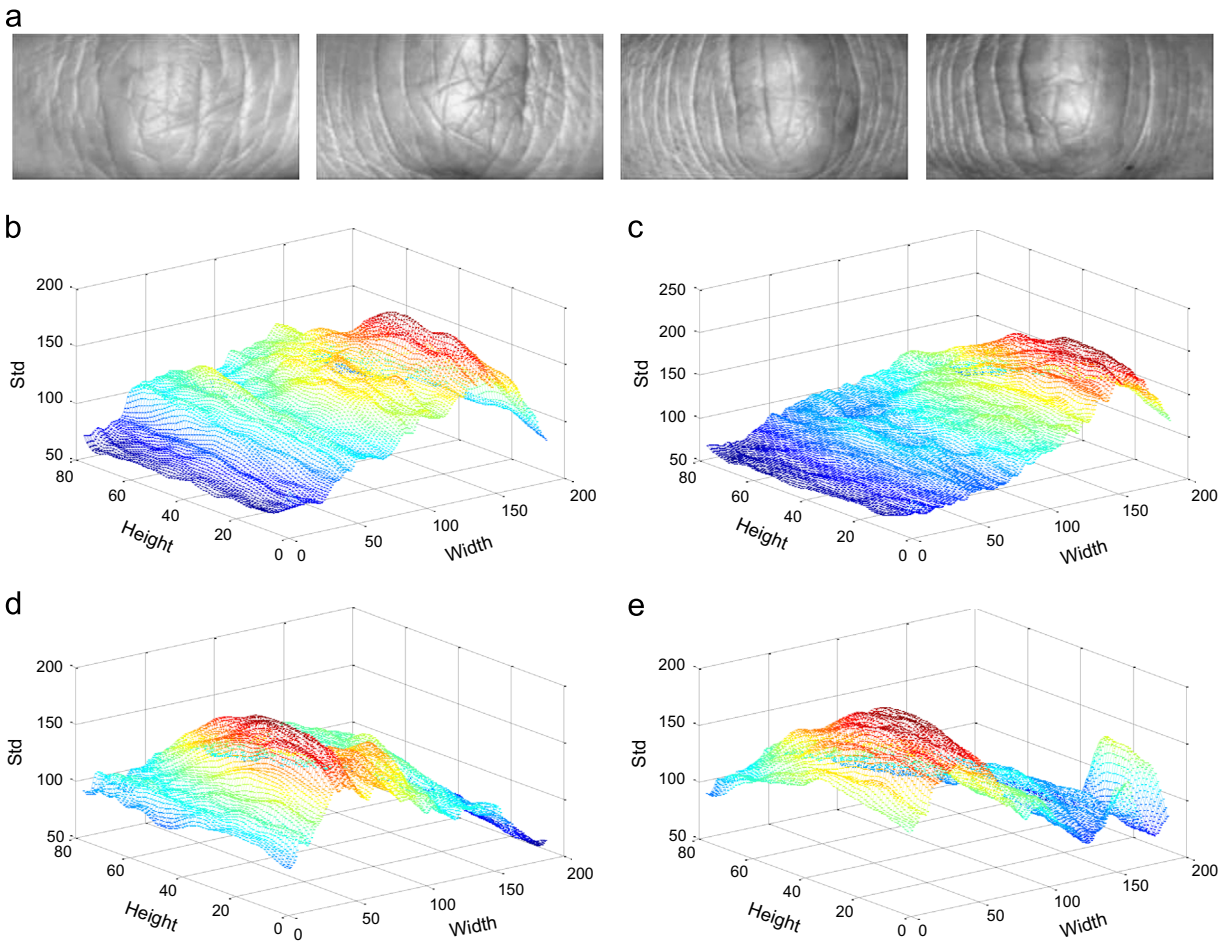

Fig. 10. (a) Four FKP ROI images from four types of finger types; the visualization of std for (b) left index; (c) left middle; (d) right index; and (e) right middle.

incorporated for efficient matching. The score level fusion scheme is used to get our final matching score. Extensive experimental results demonstrated that the proposed integration scheme performs better than existing state-of-the-art methods.

Acknowledgment

The authors would like to thank the editor and the anonymous reviewers for their critical and constructive comments and suggestions. This work was partially supported by the National Science Fund for Distinguished Young Scholars under Grant Nos. 61125305, 61233011 and 61373063, the Key Project of Chinese Ministry of Education under Grant No. 313030, and the 973 Program No. 2014CB349303.

References

[1] D. Zhang, W.K. Kong, J. You, M. Wong, Online palmprint identification, IEEE Trans. Pattern Anal. Mach. Intell. 25 (9 (September)) (2003) 1041–1050.
[2] W. K. Kong, D. Zhang, Competitive coding scheme for palmprint verification. In: Proceedings of IEEE International Conference on Image Processing, 2004, pp. 520–523.
[3] A. Kong, D. Zhang, M. Kamel, A survey of palmprint recognition, Pattern Recognit. 42 (7 (July)) (2009) 1408–1418.
[4] D. Zhang, G. Lu, W. Li, L. Zhang, N. Luo, Palmprint recognition using 3-D information, IEEE Trans. Syst. Man Cybern. Part C: Appl. Rev. 39 (5 (September)) (2009) 505–519.
[5] Z. Sun, T. Tan, Y. Wang, S.Z. Li, Ordinal palmprint representation for personal identification, IEEE Comput. Vis. Pattern Recognit. (2005) 279–284.
[6] Z. Guo, D. Zhang, L. Zhang, W. Zuo, Palmprint verification using binary orientation co-occurrence vector, Pattern Recognit. Lett. 30 (13 (October)) (2009) 1219–1227.
[7] A.K. Jain, J. Feng, Latent palmprint matching, IEEE Trans. Pattern Anal. Mach. Intell. 31 (6 (June)) (2009) 1032–1047.
[8] W. Jia, D. Huang, D. Zhang, Palmprint verification based on principal lines, Pattern Recognit. 41 (4 (April)) (2008) 1316–1328.
[9] W. Jia, D. Huang, D. Zhang, Palmprint verification based on robust line orientation code, Pattern Recognit. 41 (5 (May)) (2008) 1504–1513.
[10] X. Wu, D. Zhang, K. Wang, Fisherpalms based palmprint recognition, Pattern Recognit. Lett. 24 (15 (November)) (2003) 2829–2838.
[11] Hongyu Lin Zhang, Li, Junyu Niu, Fragile bits in palmprint recognition, IEEE Signal Process. Lett. 19 (10 (October)) (2012) 663–666.
[12] Lin Zhang, Hongyu Li, Encoding local image patterns using Riesz transforms: with applications to palmprint and finger-knuckle-print recognition, Image Vis.Comput. 30 (12 (December)) (2012) 1043–1051.
[13] R. Sanchez-Reillo, C. Sanchez-Avila, A. Gonzalez-Marcos, Biometric identification through hand geometry measurements, IEEE Trans. Pattern Anal. Mach. Intell. 22 (10 (October)) (2000) 1168–1171.
[14] L. Hong, Y. Wan, A. Jain, Fingerprint image enhancement: algorithm and performance evaluation, IEEE Trans. Pattern Anal. Mach. Intell. 20 (8 (August)) (1998) 777–789.
[15] D. Maltoni, D. Maio, A.K. Jain, S. Prabhakar, Handbook of Fingerprint Recognition, Springer, 2003.
[16] N. Ratha, R. Bolle, Automatic Fingerprint Recognition Systems, Springer, 2004.
[17] J. Gu, J. Zhou, C. Yang, Fingerprint recognition by combining global structure and local cues, IEEE Trans. Image Process. 15 (7 (July)) (2006) 1952–1964.
[18] Q. Zhao, D. Zhang, L. Zhang, N. Luo, Adaptive fingerprint pore modeling and extraction, Pattern Recognit. 43 (8 (August)) (2010) 2833–2844.
[19] J.G. Wang, W.Y. Yau, A. Suwandy, E. Sung, Personal recognition by fusing palmprint and palm vein images based on Lapacianpalm representation, Pattern Recognit. 41 (5 (May)) (2008) 1514–1527.
[20] L. Zhang, L. Zhang, D. Zhan, Finger-knuckle-print: a new biometric identifier. In: Proceedings of IEEE International Conference on Image Processing, 2009, pp. 1981–1984.
[21] L. Zhang, L. Zhang, D. Zhang, H. Zhu, Online finger-knuckle-print verification for personal authentication, Pattern Recognit. 43 (7 (July)) (2010) 2560–2571.
[22] L. Zhang, L. Zhang, D. Zhang, Finger-knuckle-print verification based on band-limited phase-only correlation. In: Proceedings of International Conference on Computer Analysis of Images and Patterns, September 2009, pp. 141–148.
[23] L. Zhang, L. Zhang, D. Zhang, H. Zhu, Ensemble of local and global information for finger-knuckle-print recognition, Pattern Recognit. 44 (9 (September)) (2011) 1990–1998.
[24] L. Zhang, L. Zhang, D. Zhang, Z. Guo, Phase congruency induced local features for finger-knuckle-print recognition, Pattern Recognit. 45 (7 (July)) (2012) 2522–2531.
[25] A. Morales, C.M. Travieso, M.A. Ferrer, J.B. Alonso, Improved finger-knuckle-print authentication based on orientation enhancement, Electron. Lett. 47 (6 (March)) (2011) 380–381.
[26] Zichao Li, Kuanquan Wang, Wangmeng Zuo, Finger-knuckle-print recognition using local orientation feature based on steerable filter. In: Proceedings of International Conference on Intelligent Computing, 2012, pp. 224–230.
[27] D.L. Woodard, P.J. Flynn, Finger surface as a biometric identifier, Computer. Vis. Image Underst. 100 (3 (December)) (2005) 357–384.
[28] A. Kumar, C. Ravikanth, Personal authentication using finger knuckle surface, IEEE Trans. Inf. Forensics Secur. 4 (1 (March)) (2009) 98–109.
[29] A Meraoumia, S Chitroub, A Bouridane, Palmprint and finger-knuckle-print for efficient person recognition based on log-Gabor filter response, Analog Integr. Circuits Signal Process. 69 (1 (October)) (2011) 17–27.
[30] T. Ojala, M. Pietikäinen, T.T. Mäenpää, Multiresolution gray-scale and rotation invariant texture classification with Local Binary Pattern, IEEE Trans. Pattern Anal. Mach. Intell. 24 (7 (July)) (2002) 971–987.
[31] PolyU Finger-Knuckle-Print Database ⟨http://www.comp.polyu.edu.hk/~biometrics⟩, 2010.
[32] M. Luessi, M. Eichmann, G. Schuster, A. Katsaggelos, Framework for efficient optimal multilevel image thresholding, J. Electron. Imag. 18 (1 (February)) (2009).
[33] T. Ahonen, A. Hadid, M. Pietikäinen, Face description with local binary patterns: application to face recognition, IEEE Trans. Pattern Anal. Mach. Intell. 28 (12 (December)) (2006) 2037–2041.
[34] G. Zhao, M. Pietikäinen, Dynamic texture recognition using Local Binary Patterns with an applic ation to facial expressions, IEEE Trans. Pattern Anal. Mach. Intell. 29 (6) (2007) 915–928.
[35] X. Huang, S. Z. Li, Y. Wang, Shape localization based on statistical method using extended local binary pattern. In: Proceedings of International Conference on Image and Graphics, 2004, pp.184–187.
[36] Wenchao Zhang, Shiguang Shan, Wen Gao, Hongming Zhang, Local Gabor Binary Pattern Histogram Sequence (LGBPHS): a novel non-statistical model for face representation and recognition. In: International Conference on Computer Vision (ICCV2005), Beijing, October 2005, pp. 786–791.
[37] R. Snelick, U. Uludag, A. Mink, M. Indovina, A.K. Jain, Large-scale evaluation of multimodal biometric authentication using state-of-the-art systems, IEEE Trans. Pattern Anal. Mach. Intell. 27 (3 (March)) (2005) 450–455.
[38] J. Daugman, The importance of being random: statistical principles of iris recognition, Pattern Recognit. 36 (2 (February)) (2003) 279–291.

Guangwei Gao received the B.S. in information and computation science from Nanjing Normal University, Nanjing, China, in 2009. He is currently pursuing Ph.D. degree from the School of Computer Science and Engineering, Nanjing University of Science and Technology, Nanjing, China. From March 2011 to September 2011 and February 2013 to August 2013, he was a exchange student of Department of Computing, Hong Kong Polytechnic University. His current research interests include face recognition, face image super-resolution and biometrics.

Jian Yang received the BS degree in mathematics from the Xuzhou Normal University in 1995. He received the M.S. degree in applied mathematics from the Changsha Railway University in 1998 and the Ph.D. degree from the Nanjing University of Science and Technology (NUST), on the subject of pattern recognition and intelligence systems in 2002. In 2003, he was a postdoctoral researcher at the University of Zaragoza. From 2004 to 2006, he was a Postdoctoral Fellow at Biometrics Centre of Hong Kong Polytechnic University. From 2006 to 2007, he was a Postdoctoral Fellow at Department of Computer Science of New Jersey Institute of Technology. Now, he is a professor in the School of Computer Science and Technology of NUST. He is the author of more than 80 scientific papers in pattern recognition and computer vision. His journal papers have been cited more than 1800 times in the ISI Web of Science, and 3000 times in the Web of Scholar Google. His research interests include pattern recognition, computer vision and machine learning. Currently, he is an associate editor of Pattern Recognition Letters and IEEE Transactions on Neural Networks and Learning Systems, respectively.

Jianjun Qian received the B.S. and M.S. degrees in 2007 and 2010, respectively. Currently, he is pursuing the Ph. D. degree at the School of Computer Science and Engineering, Nanjing University of Science and Technology (NUST), Nanjing, China. His research interests include pattern recognition, computer vision and especially focus on face recognition.

Lin Zhang received the B.S. and M.S. degrees from the Department of Computer Science and Engineering, Shanghai Jiao Tong University, Shanghai, PR China, in 2003 and 2006, respectively. He received the Ph.D. degree from the Department of Computing, The Hong Kong Polytechnic University, Hong Kong, in 2011. From March 2011 to August 2011, he was a Research Assistant with the Department of Computing, the Hong Kong Polytechnic University. He is now an Assistant Professor in School of Software Engineering, Tongji University, Shanghai, PR China. His research interests include biometrics, pattern recognition, computer vision, and perceptual image/video quality assessment, etc.